

Solution of the time-harmonic Maxwell equations using discontinuous Galerkin methods

V. Dolean^{a,b,*}, H. Fol^b, S. Lanteri^b, R. Perrussel^b

^a*Université de Nice Sophia-Antipolis, Laboratoire J.-A. Dieudonné, Parc Valrose, 06902 Nice Cedex 02*

^b*INRIA Sophia-Antipolis, 2004 rte des Lucioles, 06902 Sophia-Antipolis Cedex*

Abstract

We present numerical results concerning the solution of the time-harmonic Maxwell equations discretized by discontinuous Galerkin methods. In particular, a numerical study of the convergence, which compares different strategies proposed in the literature for the elliptic Maxwell equations, is performed in the two-dimensional case.

Key words: time-harmonic Maxwell's equations, discontinuous Galerkin methods.

1 Introduction

This work is concerned with the numerical solution of the time-harmonic Maxwell equations discretized by discontinuous Galerkin methods on unstructured meshes. Our motivation for using a discontinuous Galerkin method is the enhanced flexibility compared to the conforming edge element method [12]: for instance, dealing with non-conforming meshes is straightforward and the choice of the local approximation space is not constrained. Nonetheless, before taking full advantage of these features, it is required to carefully study the basic ingredients of the method such as the choice of the numerical flux at the interface between neighboring elements. In the context of time-harmonic

* Corresponding author.

Email addresses: dolean@math.unice.fr (V. Dolean), Hugo.Fol@inria.fr (H. Fol), Stephane.Lanteri@inria.fr (S. Lanteri), Ronan.Perrussel@inria.fr (R. Perrussel).

problems, the design of efficient solution strategies for the resulting sparse linear systems is an equally important question.

Previous works have shown convergence results for discontinuous Galerkin methods applied to the time-harmonic Maxwell equations, studied in the form of second-order vector wave equations. Most of these works use a mixed formulation [13,11] but discontinuous Galerkin methods on the non-mixed formulation have recently been proved to converge (interior penalty technique [10,1] as well as the local discontinuous Galerkin method [1]). The convergence properties of these methods in the time-domain case have been studied in [6] when using a centered flux and in [9] when using an upwind flux. The case of the upwind flux has been analyzed in [8] and [7] for the time-harmonic problems and the convergence has been proved only for a perturbed problem. The general case of Friedrichs systems and the elliptic Maxwell equations in particular has been treated in [4] and [5]. However, to our knowledge, no direct convergence analysis on the first-order time-harmonic system (1) has been conducted so far, which should be useful, for instance, when using an upwind flux (see subsection 2.3). The main contribution of this work is a numerical study of the convergence of discontinuous Galerkin methods based on centered and upwind fluxes applied to the first-order time-harmonic Maxwell system in the two-dimensional case.

The paper is organized as follows: in section 2 we present the discretization method as well as the different kind of fluxes considered. In section 3, the convergence properties are recalled in the case of the elliptic Maxwell equations and the solvability of the discrete perturbed problem is analyzed in the case of the centered flux. In section 4 the numerical convergence is studied and confronted to the theoretical convergence order. Different numerical fluxes are then compared on two distinct examples.

2 Discretization of the first-order time-harmonic Maxwell system

2.1 Formulation of the continuous problem

The system of non-dimensionalized time-harmonic Maxwell's equations can be written in the following form:

$$\begin{cases} i\omega\varepsilon_r\mathbf{E} - \text{curl } \mathbf{H} = -\mathbf{J}, \\ i\omega\mu_r\mathbf{H} + \text{curl } \mathbf{E} = 0, \end{cases} \quad (1)$$

where \mathbf{E} and \mathbf{H} are the unknown electric and magnetic fields and \mathbf{J} is a known current source. The parameters ε_r and μ_r are respectively the complex-valued

relative dielectric permittivity (integrating the electric conductivity) and the relative magnetic permeability; we consider here the case of linear isotropic media. The angular frequency of the problem is given by ω . We solve Equations (1) in a bounded domain Ω , and on its boundary $\partial\Omega = \Gamma_a \cup \Gamma_m$, we impose the following boundary conditions:

- a perfect electric conductor condition on Γ_m , ie: $\mathbf{n} \times \mathbf{E} = 0$ on Γ_m ,
 - a Silver-Müller (first-order absorbing boundary) condition on Γ^a , ie: (2)
- $$\mathbf{n} \times \mathbf{E} + \mathbf{n} \times (\mathbf{n} \times \mathbf{H}) = \mathbf{n} \times \mathbf{E}^{\text{inc}} + \mathbf{n} \times (\mathbf{n} \times \mathbf{H}^{\text{inc}}) \text{ on } \Gamma_a.$$

The vectors \mathbf{E}^{inc} and \mathbf{H}^{inc} represent the components of an incident electromagnetic wave. We can further rewrite (1)+(2), assuming \mathbf{J} equals to 0, under the following form:

$$\begin{cases} i\omega G_0 \mathbf{W} + G_x \partial_x \mathbf{W} + G_y \partial_y \mathbf{W} + G_z \partial_z \mathbf{W} = 0 \text{ in } \Omega, \\ (M_{\Gamma_m} - G_{\mathbf{n}}) \mathbf{W} = 0 \text{ on } \Gamma_m, \\ (M_{\Gamma_a} - G_{\mathbf{n}})(\mathbf{W} - \mathbf{W}_{\text{inc}}) = 0 \text{ on } \Gamma_a. \end{cases} \quad (3)$$

where $\mathbf{W} = \begin{pmatrix} \mathbf{E} \\ \mathbf{H} \end{pmatrix}$ is the new unknown vector and $G_0 = \begin{pmatrix} \varepsilon_r I_3 & 0_{3 \times 3} \\ 0_{3 \times 3} & \mu_r I_3 \end{pmatrix}$. Denoting by $(\mathbf{e}^x, \mathbf{e}^y, \mathbf{e}^z)$ the canonical basis of \mathbb{R}^3 , the matrices G_l with $l \in \{x, y, z\}$ are given by:

$$G_l = \begin{pmatrix} 0_{3 \times 3} & N \mathbf{e}^l \\ N^t \mathbf{e}^l & 0_{3 \times 3} \end{pmatrix} \text{ where for a vector } \mathbf{n}, N \mathbf{n} = \begin{pmatrix} 0 & \mathbf{n}_z & -\mathbf{n}_y \\ -\mathbf{n}_z & 0 & \mathbf{n}_x \\ \mathbf{n}_y & -\mathbf{n}_x & 0 \end{pmatrix}.$$

In the following we denote by $G_{\mathbf{n}}$ the sum $G_x \mathbf{n}_x + G_y \mathbf{n}_y + G_z \mathbf{n}_z$ and by $G_{\mathbf{n}}^+$ and $G_{\mathbf{n}}^-$ its positive and negative parts¹. We also define $|G_{\mathbf{n}}| = G_{\mathbf{n}}^+ - G_{\mathbf{n}}^-$. In order to take into account the boundary conditions, the matrices M_{Γ_m} and M_{Γ_a} are given by:

$$M_{\Gamma_m} = \begin{pmatrix} 0_{3 \times 3} & N \mathbf{n} \\ -N^t \mathbf{n} & 0_{3 \times 3} \end{pmatrix} \text{ and } M_{\Gamma_a} = |G_{\mathbf{n}}|.$$

See [3] for further details on the derivation of this formulation.

¹ If $G_{\mathbf{n}} = T \Lambda T^{-1}$ is the eigenfactorization then $G_{\mathbf{n}}^{\pm} = T \Lambda^{\pm} T^{-1}$ where Λ^+ (resp. Λ^-) only gathers the positive (resp. negative) eigenvalues.

2.2 Discretization

Let Ω_h denote a discretization of the domain Ω into a union of conforming elements (tetrahedral or hexahedral elements)

$$\bar{\Omega}_h = \bigcup_{K \in \mathcal{T}_h} K.$$

We look for the approximate solutions $\mathbf{W}_h = \begin{pmatrix} \mathbf{E}_h \\ \mathbf{H}_h \end{pmatrix}$ of (3) in $V_h \times V_h$ where the function space V_h is defined by:

$$V_h = \left\{ \mathbf{V} \in [L^2(\Omega)]^3 / \forall K \in \mathcal{T}_h, \mathbf{V}|_K \in \mathcal{P}(K) \right\}. \quad (4)$$

The term $\mathcal{P}(K)$ denotes a space of polynomial functions on the element K . We take the scalar product of the first equation of (3) by a sufficiently smooth vector field \mathbf{V} and we integrate over an element K of the mesh \mathcal{T}_h :

$$\int_K i\omega (G_0 \mathbf{W})^t \bar{\mathbf{V}} dx + \int_K \left(\sum_{l \in \{x,y,z\}} G_l \partial_l \mathbf{W} \right)^t \bar{\mathbf{V}} dx = 0.$$

By using Green's formula we obtain a weak formulation involving a boundary term. This term is replaced in discontinuous Galerkin methods by a function $\Phi_{\partial K}$ which is usually referred as the numerical flux (see also Ern and Guermond [4,5]); the aim is then to determine \mathbf{W}_h in $V_h \times V_h$ such that:

$$\int_K i\omega (G_0 \mathbf{W}_h)^t \bar{\mathbf{V}} dx - \int_K \mathbf{W}_h^t \left(\sum_{l \in \{x,y,z\}} G_l \partial_l \bar{\mathbf{V}} \right) dx + \int_{\partial K} (\Phi_{\partial K}(\mathbf{W}_h))^t \bar{\mathbf{V}} = 0, \quad \forall \mathbf{V} \in V_h \times V_h. \quad (5)$$

In order to couple the element K with its neighbors for ensuring the consistency of the discretization, this numerical flux can be defined in the following way:

$$\Phi_{\partial K}(\mathbf{W}_h) = \begin{cases} I_{FK} S_F[\mathbf{W}_h] + I_{FK} G \mathbf{n}_F \{ \mathbf{W}_h \} & \text{if } F \in \Gamma^0, \\ \frac{1}{2} (M_{F,K} + I_{FK} G \mathbf{n}_F) \mathbf{W}_h & \text{if } F \in \Gamma^m, \\ \frac{1}{2} (M_{F,K} + I_{FK} G \mathbf{n}_F) \mathbf{W}_h - \frac{1}{2} (M_{F,K} - I_{FK} G \mathbf{n}_F) \mathbf{W}^{\text{inc}} & \text{if } F \in \Gamma^a, \end{cases} \quad (6)$$

where Γ^0 , Γ^a and Γ^m respectively denote the set of interior faces, the set of faces on Γ_a and the set of faces on Γ_m . I_{FK} stands for the incidence matrix

between oriented faces and elements whose entries are given by:

$$I_{FK} = \begin{cases} 0 & \text{if the face } F \text{ does not belong to element } K, \\ 1 & \text{if } F \in K \text{ and their orientations match,} \\ -1 & \text{if } F \in K \text{ and their orientations do not match.} \end{cases}$$

We also define respectively the jump and the average of \mathbf{V} on a face F shared by two elements K and \tilde{K} :

$$\llbracket \mathbf{V} \rrbracket = I_{FK} \mathbf{V}_K + I_{F\tilde{K}} \mathbf{V}_{\tilde{K}} \text{ and } \{\mathbf{V}\} = \frac{1}{2}(\mathbf{V}_K + \mathbf{V}_{\tilde{K}}).$$

Finally, the matrix S_F allows to penalize the jump of a field or of some components of this given field on the face F and the matrix $M_{F,K}$ to be defined later insures the asymptotic consistency with the boundary conditions of the continuous problem.

2.3 Choice of the numerical flux

In this study, we aim at comparing the properties of three classical numerical fluxes:

- **a centered flux** (see [6] for the time-domain equivalent). In this case $S_F = 0$ for all the faces F and, for the boundary faces, we use:

$$M_{F,K} = \begin{cases} I_{FK} \begin{pmatrix} 0_{3 \times 3} & N \mathbf{n}_F \\ -N^t \mathbf{n}_F & 0_{3 \times 3} \end{pmatrix} & \text{if } F \in \Gamma^m, \\ |G \mathbf{n}_F| & \text{if } F \in \Gamma^a. \end{cases}$$

- **an upwind flux** (see [4,14]). In this case:

$$S_F = \begin{pmatrix} \alpha_F^E N \mathbf{n}_F N^t & 0_{3 \times 3} \\ 0_{3 \times 3} & \alpha_F^H N^t \mathbf{n}_F N \end{pmatrix}, \quad M_{F,K} = \begin{pmatrix} \eta_F N \mathbf{n}_F N^t & I_{FK} N \mathbf{n}_F \\ -I_{FK} N^t \mathbf{n}_F & 0_{3 \times 3} \end{pmatrix} \quad \forall F \in \Gamma^m,$$

with α_F^E , α_F^H and η_F equals to 1/2 for homogeneous media. The definition of M_{FK} for F in Γ^a is identical to the centered case.

- **a partially penalized upwind flux** (local Discontinuous Galerkin method, see [2]). This flux is characterized by a penalization coefficient given by:

$$S_F = \tau_F h_F^{-1} \begin{pmatrix} N \mathbf{n}_F N^t & 0 \\ 0 & 0 \end{pmatrix}, \quad M_{F,K} = \begin{pmatrix} \eta_F h_F^{-1} N \mathbf{n}_F N^t & I_{FK} N \mathbf{n}_F \\ -I_{FK} N^t \mathbf{n}_F & 0_{3 \times 3} \end{pmatrix} \quad \forall F \in \Gamma^m.$$

The definition of M_{FK} for F in Γ^a is also identical to the centered case.

3 Convergence properties of the discretized problem

We are interested in assessing these numerical fluxes for the discretization of (3). Firstly, we want the best asymptotic convergence order in L^2 -norm for the electric and magnetic field for a fixed polynomial order approximation on an unstructured mesh. Secondly, a minimal numerical dispersion is also needed. In the following we will focus on the first criterion. The asymptotic convergence order in L^2 -norm between the exact solution (\mathbf{E}, \mathbf{H}) and the approximate solution $(\mathbf{E}_h, \mathbf{H}_h)$ corresponds to the largest real coefficients β and γ such that:

$$\exists C_1, C_2, h_0 > 0, \forall h > h_0, \|\mathbf{E} - \mathbf{E}_h\|_{L^2(\Omega)} \leq C_1 h^\beta \text{ and } \|\mathbf{H} - \mathbf{H}_h\|_{L^2(\Omega)} \leq C_2 h^\gamma, \quad (7)$$

where h is the mesh size. Let us note that in the numerical examples proposed in Section 4, we will often equivalently consider the evolution of the norm of the error against the square root of the number of degrees of freedom (dofs), in order to deduce coefficients β and γ .

We first recall in Table 1 below the theoretical convergence order for the elliptic Maxwell equations [4,5], for a sufficiently smooth solution and when the local function space $\mathcal{P}(K)$ is $[P_k(K)]^3$ i.e. the space of vectors whose components are polynomials of order at most k . When using the flux with a penalization of \mathbf{E} , similar convergence results are proved for the time-harmonic Maxwell equations in [1].

flux	centered	upwind	penalization of \mathbf{E}
field \mathbf{E}	k	$k + 1/2$	$k + 1$
field \mathbf{H}	k	$k + 1/2$	k

Table 1

Theoretical convergence order for the elliptic Maxwell equations.

3.1 Solution of the discretized perturbed problem

A few comments need to be stated concerning the convergence properties of such a scheme applied to the first-order formulation of the time-harmonic Maxwell equations. First of all, the case of the upwind flux has been analyzed in [8] for the perturbed Maxwell problem, that is when $i\omega$ is replaced by

$\nu + i\omega$ with ν a strictly positive parameter. For a sufficiently regular solution the norm of the error behaves as $h^{p+1/2}$ where h is the mesh parameter.

The case of the centered flux has been studied in [6] for the time-domain Maxwell equations and in this case the norm of the error behaves as h^p where h is the mesh parameter. For the time-harmonic equations no convergence proofs are available so far. We can only study here the solvability of the discrete problem in the case of a perturbed problem (we replace $i\omega$ by $i\omega + \nu$ with $\nu > 0$) following an idea used by Helluy [7] in the case of the upwind flux. In the case of the perturbed problem and assuming homogeneous boundary conditions, the formulation can be simply written as:

$$\begin{cases} \text{Find } \mathbf{W}_h \text{ in } V_h \times V_h \text{ such that:} \\ a(\mathbf{W}_h, \mathbf{V}) + b(\mathbf{W}_h, \mathbf{V}) = 0, \quad \forall \mathbf{V} \in V_h \times V_h, \end{cases} \quad (8)$$

with, $\forall \mathbf{U}, \mathbf{V} \in V_h \times V_h$:

$$\begin{aligned} a(\mathbf{U}, \mathbf{V}) &= \int_{\Omega_h} ((i\omega + \nu)G_0 \mathbf{U})^t \bar{\mathbf{V}} dv + \sum_{F \in \Gamma^a} \int_F \left(\frac{1}{2} |G \mathbf{n}_F| \mathbf{U} \right)^t \bar{\mathbf{V}} ds \\ &+ \sum_{F \in \Gamma^m} \int_F \left(\frac{1}{2} M_{F,K} \mathbf{U} \right)^t \bar{\mathbf{V}} ds + \sum_{F \in \Gamma^0} \int_F (S_F [\mathbf{U}])^t \llbracket \bar{\mathbf{V}} \rrbracket_F ds, \end{aligned} \quad (9)$$

and:

$$\begin{aligned} b(\mathbf{U}, \mathbf{V}) &= \sum_{K \in \mathcal{T}_h} \int_K \left(\sum_{l \in \{x,y,z\}} G_l \partial_l (\mathbf{U}) \right)^t \bar{\mathbf{V}} dv \\ &- \sum_{F \in \Gamma^a \cup \Gamma^m} \int_F \left(\frac{1}{2} I_{FK} G \mathbf{n}_F \mathbf{U} \right)^t \bar{\mathbf{V}} ds \\ &- \sum_{F \in \Gamma^0} \int_F (G \mathbf{n}_F \llbracket \mathbf{U} \rrbracket)^t \{ \bar{\mathbf{V}} \} ds. \end{aligned} \quad (10)$$

We have the following result:

PROPOSITION 1 *The solution of problem (8) is null.*

Proof First, considering the fact that the matrices $|G \mathbf{n}_F|$, S_F , $\Re(G_0)$ and $-\Im(G_0)$ are hermitian and denoting by $\mathcal{H}(M_{F,K})$ the hermitian part of $M_{F,K}$

for F in Γ^m , which is equal to $\begin{pmatrix} \eta_F N \mathbf{n}_F N^t & 0_{3 \times 3} \\ 0_{3 \times 3} & 0_{3 \times 3} \end{pmatrix}$, one has:

$$\begin{aligned}
\Re(a(\mathbf{W}_h, \mathbf{W}_h)) &= \int_{\Omega_h} ((\nu \Re(G_0) - \omega \Im(G_0)) \mathbf{W}_h)^t \overline{\mathbf{W}_h} dv \\
&+ \sum_{F \in \Gamma^0} \int_F (S_F \llbracket \mathbf{W}_h \rrbracket)^t \llbracket \overline{\mathbf{W}_h} \rrbracket_F ds \\
&+ \sum_{F \in \Gamma^a} \int_F \left(\frac{1}{2} |G \mathbf{n}_F| \mathbf{W}_h \right)^t \overline{\mathbf{W}_h} ds \\
&+ \sum_{F \in \Gamma^m} \int_F \left(\frac{1}{2} \mathcal{H}(M_{F,K}) \mathbf{W}_h \right)^t \overline{\mathbf{W}_h} ds.
\end{aligned} \tag{11}$$

Then, we rewrite using the corresponding Green identity an equivalent expression of the sesquilinear form b :

$$\begin{aligned}
b(\mathbf{U}, \mathbf{V}) &= - \sum_{K \in \mathcal{T}_h} \left[\int_K \mathbf{U}^t \left(\sum_{l \in \{x,y,z\}} G_l \partial_l(\overline{\mathbf{V}}) \right) dv - \right. \\
&\quad \left. \sum_{F \in \partial K} \int_F (I_{FK} G \mathbf{n}_F \mathbf{U}|_K)^t \mathbf{V}|_K ds \right] \\
&- \sum_{F \in \Gamma^a} \int_F \left(\frac{1}{2} I_{FK} G \mathbf{n}_F \mathbf{U} \right)^t \overline{\mathbf{V}} ds \\
&- \sum_{F \in \Gamma^0} \int_F (G \mathbf{n}_F \llbracket \mathbf{U} \rrbracket)^t \{ \overline{\mathbf{V}} \} ds, \quad \forall \mathbf{U}, \mathbf{V} \in V_h \times V_h.
\end{aligned} \tag{12}$$

By noticing that on a face $F \in \Gamma^0$ separating two elements K and \tilde{K} :

$$\begin{aligned}
(G \mathbf{n}_F \{ \mathbf{U} \})^t \llbracket \mathbf{V} \rrbracket + (G \mathbf{n}_F \llbracket \mathbf{U} \rrbracket)^t \{ \mathbf{V} \} &= (I_{FK} G \mathbf{n}_F \mathbf{U}|_K)^t \mathbf{V}|_K \\
&+ (I_{F\tilde{K}} G \mathbf{n}_F \mathbf{U}|_{\tilde{K}})^t \mathbf{V}|_{\tilde{K}},
\end{aligned}$$

which is in part due to the fact that $G \mathbf{n}_F$ is hermitian, one deduces:

$$\begin{aligned}
b(\mathbf{U}, \mathbf{V}) &= - \sum_{K \in \mathcal{T}_h} \int_K \mathbf{U}^t \left(\sum_{l \in \{x,y,z\}} G_l \partial_l(\overline{\mathbf{V}}) \right) dv \\
&+ \sum_{F \in \Gamma^a} \int_F \left(\frac{1}{2} I_{FK} G \mathbf{n}_F \mathbf{U} \right)^t \overline{\mathbf{V}} ds \\
&+ \sum_{F \in \Gamma^0} \int_F (G \mathbf{n}_F \{ \mathbf{U} \})^t \llbracket \overline{\mathbf{V}} \rrbracket ds, \quad \forall \mathbf{U}, \mathbf{V} \in V_h \times V_h.
\end{aligned} \tag{13}$$

Thus, it is now straightforward to see that b is anti-hermitian and conse-

quently:

$$\begin{aligned}
\Re(a(\mathbf{W}_h, \mathbf{W}_h) + b(\mathbf{W}_h, \mathbf{W}_h)) &= \int_{\Omega_h} ((\nu\Re(G_0) - \omega\Im(G_0))\mathbf{W}_h)^t \overline{\mathbf{W}_h} dv \\
&+ \sum_{F \in \Gamma^0} \int_F (S_F \llbracket \mathbf{W}_h \rrbracket)^t \llbracket \overline{\mathbf{W}_h} \rrbracket_F ds \\
&+ \sum_{F \in \Gamma^a} \int_F \left(\frac{1}{2} |G\mathbf{n}_F| \mathbf{W}_h \right)^t \overline{\mathbf{W}_h} ds \\
&+ \sum_{F \in \Gamma^m} \int_F \left(\frac{1}{2} \mathcal{H}(M_{F,K}) \mathbf{W}_h \right)^t \overline{\mathbf{W}_h} ds,
\end{aligned}$$

From (8), $\Re(a(\mathbf{W}_h, \mathbf{W}_h) + b(\mathbf{W}_h, \mathbf{W}_h))$ is also equal to zero. As $\nu\Re(G_0) - \omega\Im(G_0)$ is positive definite and $|G\mathbf{n}_F|$, S_F and $\mathcal{H}(M_{F,K})$ are positive, the vector field \mathbf{W}_h is null. \blacksquare

4 Numerical results

In the first part of this section we will present a numerical comparison of different fluxes for a very simple test case and different kind of meshes. In the second part, the results on a less trivial problem are compared to those obtained with the plane wave example.

We consider the case of an electric transverse wave in the plane (O, x, y) . In this case the components \mathbf{E}_z , \mathbf{H}_x and \mathbf{H}_y are zero. We numerically simulate the propagation of a plane wave in vacuum where the incident wave is given by $(\mathbf{E}_x^{\text{inc}}, \mathbf{E}_y^{\text{inc}}, \mathbf{H}_z^{\text{inc}}) = \exp(-i\omega x)(0, 1, 1)$. The computational domain is the unit square $\Omega =]0; 1[^2$ and a Silver-Müller boundary condition is imposed on the whole boundary, that is $\Gamma_a = \partial\Omega$ and $\Gamma_m = \emptyset$. The parameters ε_r and μ_r are set to 1 everywhere and we choose $\omega = 2\pi$. We numerically estimate the asymptotic convergence order of discontinuous Galerkin methods for the above problem using two different sequences of triangular meshes:

- **uniformly refined meshes.** The first mesh of Figure 1(a) is uniformly refined resulting in the meshes of Figures 1(b) and 1(c).
- **independent meshes.** We use four unstructured (quasi-uniform) independent meshes with an imposed maximal mesh size h (see Figure 2 for the first three meshes). These meshes are denoted by \mathcal{T}_i for $i = 1, \dots, 4$ with h in a decreasing order. Thus \mathcal{T}_{i+1} is not a refinement of \mathcal{T}_i .

Our implementation of high order discontinuous Galerkin methods makes use of nodal basis functions with equi-spaced nodes.

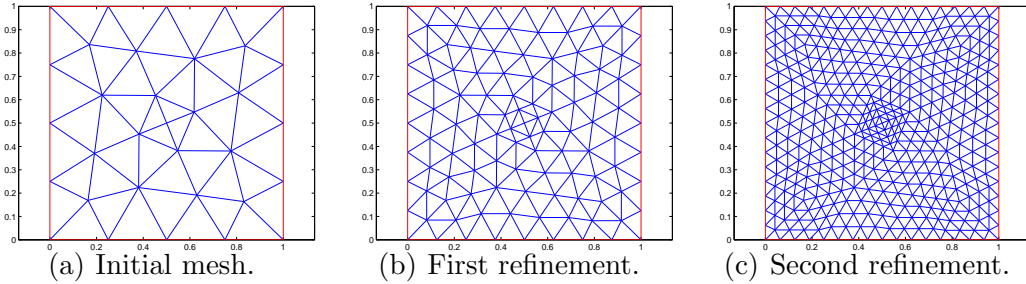


Fig. 1. Initial mesh of the unit square and two uniform refinements.

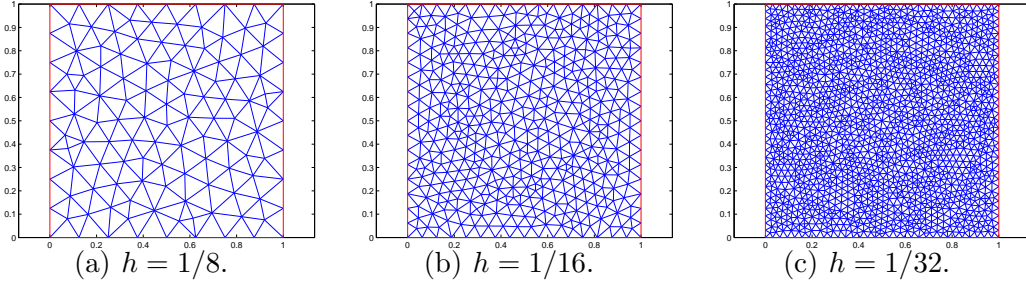
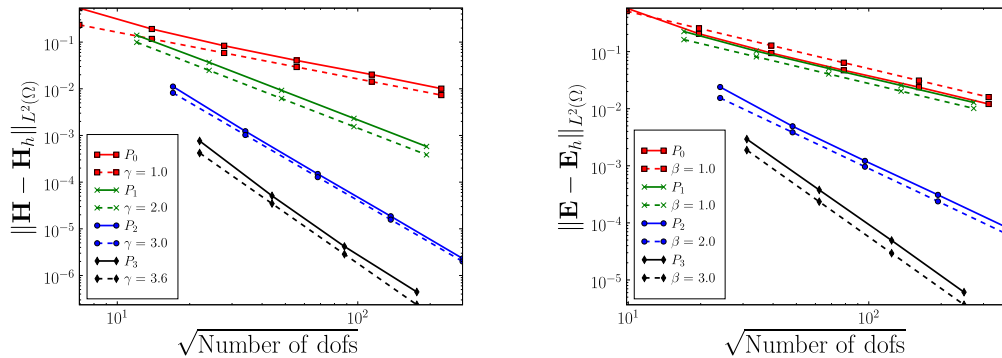


Fig. 2. First three independent unstructured meshes.

4.1 Convergence behavior using meshes obtained by uniform refinement

Centered flux. Numerical convergence results in a logarithmic scale are shown on Figure 3. They clearly demonstrate the interest of higher order polynomial approximations which allow a considerable reduction of the number of degrees of freedom to reach the same accuracy. Table 2 summarizes numerical estimates (using a linear regression method) of the asymptotic convergence order.



(a) $\|\mathbf{H} - \mathbf{H}_h\|_{L^2(\Omega)}$ against the square root of the number of dofs.

(b) $\|\mathbf{E} - \mathbf{E}_h\|_{L^2(\Omega)}$ against the square root of the number of dofs.

Fig. 3. Convergence results using a **centered flux**. Solid lines show the evolution for the whole of the numerical results and dotted lines show the asymptotic tendency, using coefficients β or γ from inequalities (7) estimated by a linear regression.

The method based on a P_0 approximation (*i.e.* the standard cell centered finite volume method) is special: the convergence order is optimal for both

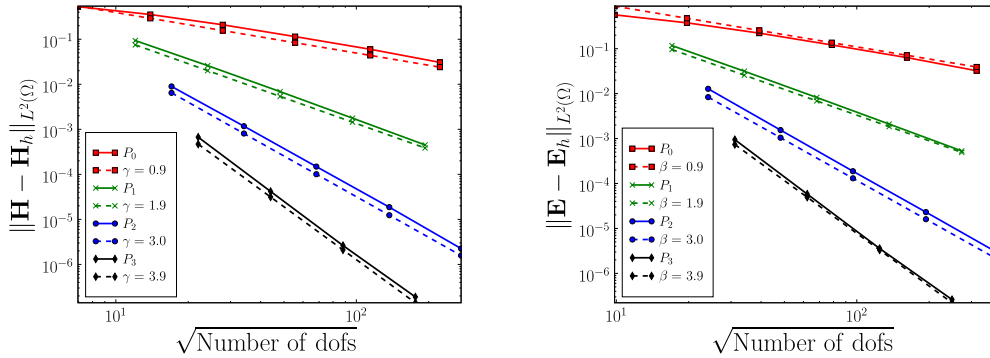
	P_0	P_1	P_2	P_3
\mathbf{E}	1.0	1.0	2.0	3.0
\mathbf{H}	1.0	2.0	3.0	3.6

Table 2

Numerical convergence order using a centered flux.

fields \mathbf{E} and \mathbf{H} , that is, equal to $k + 1$. This could be the consequence of using uniformly refined meshes, since a somewhat different behavior is obtained for independent meshes with decreasing mesh size (see subsection 4.2). For the other polynomial degrees, we get exactly the predicted theoretical convergence order in the elliptic case for \mathbf{E} , whereas for \mathbf{H} , this convergence order is optimal. Therefore, in this example, the magnetic field is better approximated than the electric field, when using the centered flux.

Upwind flux. We used here the parameters $\alpha_F^H = \alpha_F^E = \eta_F = 1$ for each face F . Numerical convergence results are shown on Figure 4. Similar conclusions can be derived as in the centered case except that the convergence properties of the methods based on P_0 and P_1 interpolations are this time clearly different with respect to the centered case. The asymptotic convergence orders (see Table 3) are similar for both fields and correspond to the theory for the elliptic Maxwell equations. The convergence is optimal except for the case P_0 , but nevertheless we are still above the theoretical estimates.



(a) $\|\mathbf{H} - \mathbf{H}_h\|_{L^2(\Omega)}$ against the square root of the number of dofs. (b) $\|\mathbf{E} - \mathbf{E}_h\|_{L^2(\Omega)}$ against the square root of the number of dofs.

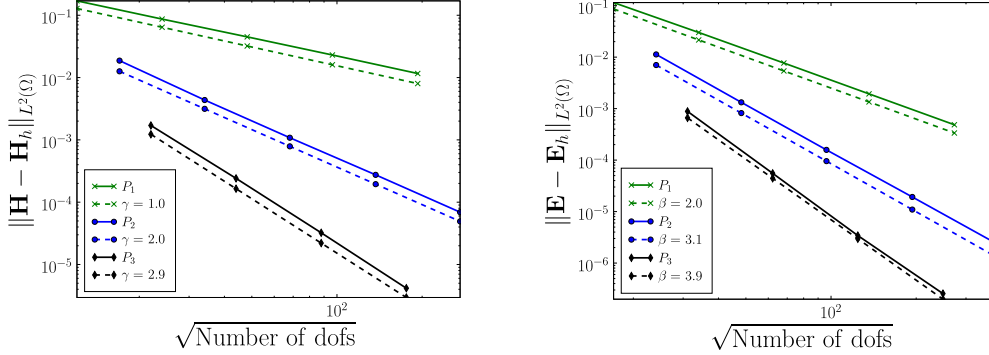
Fig. 4. Convergence results using an **upwind flux**. Solid lines show the evolution for the whole of the numerical results and dotted lines show the asymptotic tendency, using coefficients β or γ from inequalities (7) estimated by a linear regression.

	P_0	P_1	P_2	P_3
\mathbf{E}	0.9	1.9	3.0	3.9
\mathbf{H}	0.9	1.9	3.0	3.9

Table 3

Numerical convergence order using an upwind flux.

Penalized flux on \mathbf{E} . We set $\tau_F = \eta_F = 1$ for each face F . Results are shown on Figure 5. Table 4 summarizes the numerical estimates of the asymptotic convergence order. Besides the expected lack of convergence in the case P_0 , we can notice for all the other cases ($(P_k)_{k>0}$) a complementary behavior with respect to the centered flux, since this time we get an optimal convergence rate for \mathbf{E} , but not for \mathbf{H} .



(a) $\|\mathbf{H} - \mathbf{H}_h\|_{L^2(\Omega)}$ against the square root of the number of dofs. (b) $\|\mathbf{E} - \mathbf{E}_h\|_{L^2(\Omega)}$ against the square root of the number of dofs.

Fig. 5. Convergence results using a **penalized flux on \mathbf{E}** . Solid lines show the evolution for the whole of the numerical results and dotted lines show the asymptotic tendency, using coefficients β or γ from inequalities (7) estimated by a linear regression.

	P_0	P_1	P_2	P_3
\mathbf{E}	X	2.0	3.1	3.9
\mathbf{H}	X	1.0	2.0	2.9

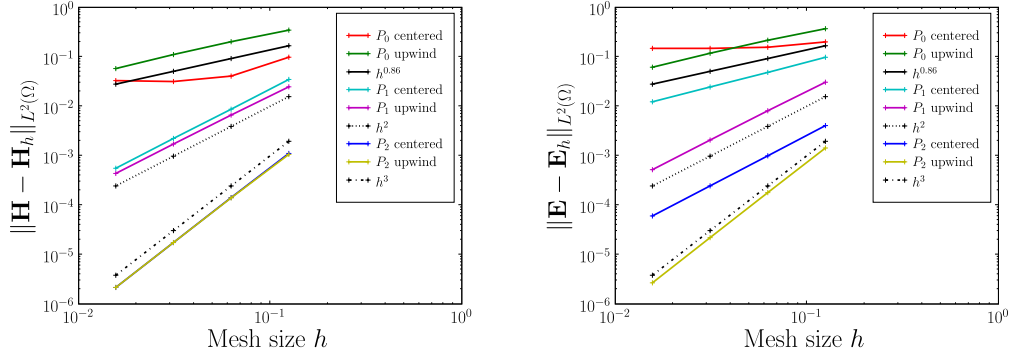
Table 4

Numerical convergence order using a penalized flux on \mathbf{E} .

4.2 Convergence behavior using independent meshes

On Figure 6, we compare the evolution of the L^2 -norm of the error with the mesh size h by using the meshes $(\mathcal{T}_i)_{i=1,\dots,4}$, for both a centered flux and an upwind flux, Figure 6(b) corresponds to the error for the field \mathbf{E} while Figure 6(a) corresponds to the error for the field \mathbf{H} . The results for the upwind flux are the same as for the uniformly refined meshes. For the centered flux, note the lack of convergence for the case P_0 . For all the other cases the results remain the same as for the uniformly refined meshes.

It is already known for time-domain problems that the centered flux combined to a leap-frog time integration scheme results in a non-dissipative discontinuous Galerkin method (a mandatory feature for long time computations, see [6]). As far as time-harmonic problems are concerned, the previous results show



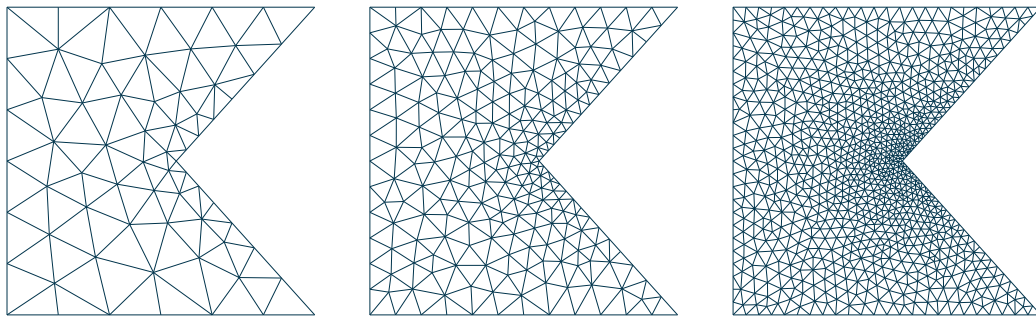
(a) $\|\mathbf{H} - \mathbf{H}_h\|_{L^2(\Omega)}$ against the mesh size h . (b) $\|\mathbf{E} - \mathbf{E}_h\|_{L^2(\Omega)}$ against the mesh size h .
 Fig. 6. Comparison of the convergence results between **centered flux** and **upwind flux**.

that the upwind flux has better convergence properties. Nevertheless, the centered flux remains less expensive both for time-domain and time-harmonic problems (arithmetic operations and memory requirements).

4.3 Numerical comparisons on a less trivial problem

The domain is the square $[-1; 1]^2$ where we have suppressed a part by inserting a point of coordinates $(0.1, 0)$ at it is shown on Figure 7. The properties ε_r and μ_r are still homogeneous and equal to one. Appropriate non-homogeneous Dirichlet boundary conditions are enforced on the boundary of the domain in order to obtain $\mathbf{E} = (\sin(2\pi y), \sin(2\pi x))^t$ as the solution.

The mesh is not fully homogeneous as it is shown on Figure 7; it is slightly denser next to the point of coordinates $(0.1, 0)$. Independent meshes have been used as in Subsection (4.2).

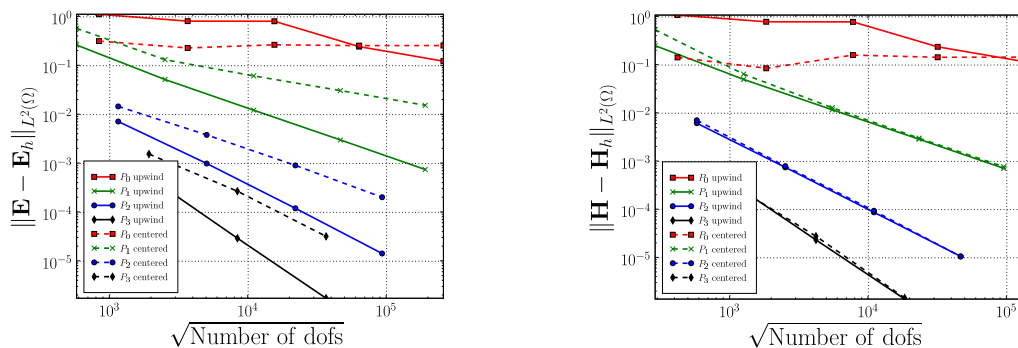


(a) First mesh. $h_{\max} = 0.32$ (b) Second mesh. $h_{\max} = 0.16$ (c) Third mesh. $h_{\max} = 0.32$

Fig. 7. Three first meshes used for the second example.

The results shown on Figure 8 are in a full agreement with those obtained in

the case of the plane wave and independent meshes at Subsection 4.2.



(a) Evolution of the L^2 -norm of the error for the \mathbf{E} field.

(b) Evolution of the L^2 -norm of the error for the \mathbf{H} field.

Fig. 8. Evolution of the L^2 -norm of the error against the square root of the number of degrees of freedom (dofs).

References

- [1] A. Buffa and I. Perugia. Discontinuous Galerkin approximation of the Maxwell eigenproblem. Technical Report PV-24, IMATI-CNR, 2005.
- [2] Bernardo Cockburn and Chi-Wang Shu. The local discontinuous Galerkin method for time-dependent convection-diffusion systems. *SIAM J. Numer. Anal.*, 35(6):2440–2463 (electronic), 1998.
- [3] Victorita Dolean, Hugo Fol, Stéphane Lanteri, and Serge Piperno. Méthodes de Galerkin Discontinu pour les équations de Maxwell en régime harmonique. Technical Report 5904, INRIA, September 2005.
- [4] Alexandre Ern and Jean-Luc Guermond. Discontinuous Galerkin Methods for Friedrichs’ systems. I. General theory. *SIAM J. Numer. Anal.*, 2006. In press.
- [5] Alexandre Ern and Jean-Luc Guermond. Discontinuous Galerkin Methods for Friedrichs’ systems. II. Second-order elliptic PDE’s. *SIAM J. Numer. Anal.*, 2006. In press.
- [6] Loula Fezoui, Stéphane Lanteri, Stéphanie Lohrengel, and Serge Piperno. Convergence and stability of a discontinuous Galerkin time-domain method for the 3D heterogeneous Maxwell equations on unstructured meshes. *M2AN Math. Model. Numer. Anal.*, 39(6):1149–1176, 2005.
- [7] P. Helluy. *Résolution numérique des équations de Maxwell harmoniques par une méthode d’éléments finis discontinus*. Thèse en mathématiques appliquées, Ecole Nationale Supérieure de l’Aéronautique, 1994.

- [8] P. Helluy and S. Dayma. Convergence d'une approximation discontinue des systèmes du premier ordre. *C. R. Acad. Sci. Paris Sér. I Math.*, 319(12):1331–1335, 1994.
- [9] J. S. Hesthaven and T. Warburton. Nodal high-order methods on unstructured grids. I. Time-domain solution of Maxwell's equations. *J. Comput. Phys.*, 181(1):186–221, 2002.
- [10] Paul Houston, Ilaria Perugia, Anna Schneebeli, and Dominik Schötzau. Interior penalty method for the indefinite time-harmonic Maxwell equations. *Numer. Math.*, 100(3):485–518, 2005.
- [11] Paul Houston, Ilaria Perugia, Anna Schneebeli, and Dominik Schötzau. Mixed discontinuous Galerkin approximation of the Maxwell operator: the indefinite case. *M2AN Math. Model. Numer. Anal.*, 39(4):727–753, 2005.
- [12] Peter Monk. *Finite element methods for Maxwell's equations*. Numerical Mathematics and Scientific Computation. Oxford University Press, New York, 2003.
- [13] I. Perugia, D. Schötzau, and P. Monk. Stabilized interior penalty methods for the time-harmonic Maxwell equations. *Comput. Methods Appl. Mech. Engrg.*, 191(41-42):4675–4697, 2002.
- [14] Serge Piperno. L^2 -stability of the upwind first order finite volume scheme for the Maxwell equations in two and three dimensions on arbitrary unstructured meshes. *M2AN Math. Model. Numer. Anal.*, 34(1):139–158, 2000.

